Extracting cavity and pulse phases from limited data for coherent pulse stacking

Yilun Xu (许逸伦)[1,2,3], Russell Wilcox[1], John Byrd[1], Lawrence Doolittle[1], Qiang Du (杜 强)[1], Gang Huang (黄 刚)[1], Yawei Yang (杨亚威)[1], Tong Zhou (周 通)[1], Lixin Yan (颜立新)[2,3,*], Wenhui Huang (黄文会)[2,3], and Chuanxiang Tang (唐传祥)[2,3]

[1]*Accelerator Technology and Applied Physics Division, Lawrence Berkeley National Laboratory, Berkeley, CA 94720, USA*

[2]*Department of Engineering Physics, Tsinghua University, Beijing 100084, China*

[3]*Key Laboratory of Particle and Radiation Imaging, Ministry of Education, Tsinghua University, Beijing 100084, China*

**Corresponding author: yanlx@tsinghua.edu.cn*

Received November 27, 2017; accepted February 7, 2018; posted online March 22, 2018

Coherent pulse stacking (CPS) is a new time-domain coherent addition technique that stacks several optical pulses into a single output pulse, enabling high pulse energy and high average power. A Z-domain model targeting the pulsed laser is assembled to describe the optical interference process. An algorithm, extracting the cavity phase and pulse phases from limited data, where only the pulse intensity is available, is developed to diagnose optical cavity resonators. We also implement the algorithm on the cascaded system of multiple optical cavities, achieving phase errors less than 1.0° (root mean square), which could ensure the stability of CPS.

OCIS codes: 070.2025, 120.5050, 140.4780, 320.0320.
doi: 10.3788/COL201816.040701.

High average power lasers are essential tools for discovery science and applications, such as laser-driven plasma wakefield acceleration (LWFA) towards future tera-electron-volt (TeV) colliders[1,2], and a megahertz (MHz) pump–probe for modern X-ray free electron laser (XFEL)[3]. The primary technical gaps between present laser capabilities and the performance required for these key applications include high average power of the kilowatt (kW) range, high wall plug efficiency, and femtosecond precise pulse timing. Fiber laser systems show promising high efficiency, excellent beam quality, and stability[4], but are limited by pulse energy. Coherent pulse stacking (CPS) is capable of conveniently adding large numbers of pulses, enabling the extraction of all available stored energy from a fiber amplifier while maintaining low intensity to minimize nonlinear effects[5–8]. Integrating CPS with spatial and spectral combining has the potential to provide joule level pulse energy at a kilohertz (kHz) repetition rate to bridge the technical gap[9–11].

CPS is a new time-domain coherent addition technique that stacks several optical pulses into a single output pulse. Coherent pulses are stacked in a traveling-wave resonant cavity (Gires–Tournois interferometer), which is composed of a partially reflecting front mirror and several completely reflecting beam-folding mirrors[12]. The initial pulses of the tailored optical pulse burst enter the reflecting resonant cavity and interfere destructively at the cavity output port, thus storing optical energy inside the resonant cavity. Later, the final pulse in the burst produces a constructive interference with the previous intracavity pulses at the output port, so that all stored energy is extracted from the resonant cavity into a single output pulse.

The efficiency of the CPS system is related to the ability to control the cavity round-trip phase accumulated by optical pulses in each path in order to guarantee the constructive interference. The round-trip phase of each cavity is stabilized against environmental perturbations and adjusted for a prescribed phase value by proper feedback control of a piezo-driven mirror. Failure of maintaining the cavity phase matching translates into a decrease of the stacking efficiency and combined peak power.

In this Letter, we proposed an algorithm in the Z domain to extract the cavity phase and pulse phases from limited data. Instead of phase stabilization techniques depending on a single detector at the system output, such as the hill-climbing algorithm [stochastic parallel gradient descent (SPGD)][13] and the dithering method [locking of optical coherence via single-detector electronic-frequency tagging(LOCSET)][14], we use all of the available information from the optical system and calculate the individual round-trip phase for each cavity accurately. Compared with the pulse-pattern-based cavity phase detection algorithm[15,16], the technique reported here eliminates the time-consuming calibration procedure (to obtain template vectors for each cavity). This pattern-free phase detection algorithm can scale to large numbers of pulses without slowing the control system.

To diagnose an optical cavity resonator, one has to derive the cavity phase from limited measurements provided by the corresponding photodiode, where only the intensity is available. This can be treated as a gray box model, which combines a partial theoretical structure with data to complete the model. We have developed a control system model describing the optical interference process in the Z domain, which gives a direct link to digital

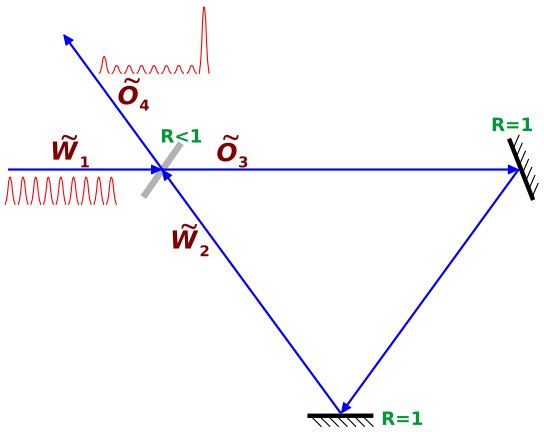

Fig. 1. Physical model of pulse interference in the Z domain.

radio frequency (RF) engineering and provides solutions to deterministic optical phase measurement and scalable feedback control.

If the round-trip length is L, the cavity round-trip optical phase shift is $\varphi = 2\pi L/\lambda_0$, where λ_0 is the optical wavelength. Z transform is employed to describe the first-order physics of a front mirror as a beam combiner/splitter, as shown in Fig. 1. We can express the delay line in the context of a pulsed laser as

$$\tilde{O}_4 = r\tilde{W}_1 + it\tilde{W}_2, \tag{1a}$$

$$\tilde{O}_3 = it\tilde{W}_1 + r\tilde{W}_2, \tag{1b}$$

$$\tilde{W}_2 = z^{-1}\alpha e^{i\varphi}\tilde{O}_3, \tag{1c}$$

where $(\tilde{W}_1, \tilde{W}_2)$ and $(\tilde{O}_3, \tilde{O}_4)$ are input and output pulse electric fields, respectively. Here, r and t are reflection and transmission coefficients, which are related by $r^2 + t^2 = 1$. The unit delay z^{-1} means that the circulating pulse travels in the cavity for a round-trip[16]. Assuming that the cavity is lossless and there is no additional loss due to imperfect interference, transmission loss coefficient α is 1. We call the round-trip phase φ the "cavity phase", which is linear with the cavity round-trip length and should be fixed within a small fraction of the optical wavelength against environmental perturbations by the feedback control.

The system transfer function $H(z)$ is therefore

$$H(z) = \frac{Y(z)}{X(z)} = \frac{r - \alpha e^{i\varphi}z^{-1}}{1 - r\alpha e^{i\varphi}z^{-1}}, \tag{2}$$

where $H(z)$ is the linear mapping of the Z transform of the input $X(z)$ to the Z transform of the output $Y(z)$. The coherent pulse stacker acts as a digital filter, which is characterized by the cavity phase φ and the front-mirror reflectivity r. The Z-domain model can be extended to cascaded cavities as easily as

$$H_{\text{cascaded}}(z) = \prod_m H_m(z). \tag{3}$$

For an ultrashort optical pulse train consisting of n pulses, we define the complex field of the k^{th} individual pulse as $A_k \cdot e^{i\psi_k}$, where A_k and ψ_k characterize the amplitude and phase. Instead of using the stack pulse train itself, a special probe pulse train can be injected together with the stack pulse train to diagnose the optical cavity fluctuation and lock the cavity phase according to the described cavity Z-domain model. Pulses are sampled with a fast photodiode, and the phase probe pulse train is triggered accordingly; then, the peak of each pulse is searched in the photodiode trace for further processing. Let us denote the input of the probe pulse train as $x(k) = {}^{\text{in}}A_k \cdot e^{i^{\text{in}}\psi_k}$, while the output is $y(k) = {}^{\text{out}}A_k \cdot e^{i^{\text{out}}\psi_k}$. Taking the Z transform of the input and output pulse trains, respectively, yields

$$X(z) = \sum_{k=1}^{n} {}^{\text{in}}A_k \cdot e^{i^{\text{in}}\psi_k} \cdot z^{-(k-1)}, \tag{4}$$

and

$$Y(z) = \sum_{k=1}^{n} {}^{\text{out}}A_k \cdot e^{i^{\text{out}}\psi_k} \cdot z^{-(k-1)}. \tag{5}$$

Combining Eqs. (2), (4), and (5) and rearranging these equations result in

$$\begin{aligned}(r - \alpha e^{i\varphi}z^{-1})\sum_{k=1}^{n} {}^{\text{in}}A_k \cdot e^{i^{\text{in}}\psi_k} \cdot z^{-(k-1)} \\ = (1 - r\alpha e^{i\varphi}z^{-1})\sum_{k=1}^{n} {}^{\text{out}}A_k \cdot e^{i^{\text{out}}\psi_k} \cdot z^{-(k-1)}.\end{aligned} \tag{6}$$

Expanding polynomials in terms of z and equating coefficients of variables with the same order on both sides in Eq. (6) give us

$$\begin{cases} r \cdot {}^{\text{in}}A_1 \cdot e^{i^{\text{in}}\psi_1} = {}^{\text{out}}A_1 \cdot e^{i^{\text{out}}\psi_1} \\ -\alpha e^{i\varphi} \cdot {}^{\text{in}}A_1 \cdot e^{i^{\text{in}}\psi_1} + r \cdot {}^{\text{in}}A_2 \cdot e^{i^{\text{in}}\psi_2} = {}^{\text{out}}A_2 \cdot e^{i^{\text{out}}\psi_2} - \alpha e^{i\varphi} \cdot r \cdot {}^{\text{out}}A_1 \cdot e^{i^{\text{out}}\psi_1} \\ \vdots \\ -\alpha e^{i\varphi} \cdot {}^{\text{in}}A_{k-1} \cdot e^{i^{\text{in}}\psi_{k-1}} + r \cdot {}^{\text{in}}A_k \cdot e^{i^{\text{in}}\psi_k} = {}^{\text{out}}A_k \cdot e^{i^{\text{out}}\psi_k} - \alpha e^{i\varphi} \cdot r \cdot {}^{\text{out}}A_{k-1} \cdot e^{i^{\text{out}}\psi_{k-1}} \\ \vdots \\ -\alpha e^{i\varphi} \cdot {}^{\text{in}}A_{n-1} \cdot e^{i^{\text{in}}\psi_{n-1}} + r \cdot {}^{\text{in}}A_n \cdot e^{i^{\text{in}}\psi_n} = {}^{\text{out}}A_n \cdot e^{i^{\text{out}}\psi_n} - \alpha e^{i\varphi} \cdot r \cdot {}^{\text{out}}A_{n-1} \cdot e^{i^{\text{out}}\psi_{n-1}} \\ {}^{\text{in}}A_n \cdot e^{i^{\text{in}}\psi_n} = r \cdot {}^{\text{out}}A_n \cdot e^{i^{\text{out}}\psi_n}. \end{cases} \tag{7}$$

For the general term formula of Eq. (7), collecting the same index pulse term on one side leads to

$$\begin{aligned}&\alpha e^{i\varphi}(r\cdot {}^{\text{out}}A_{k-1}\cdot e^{i{}^{\text{out}}\psi_{k-1}}-{}^{\text{in}}A_{k-1}\cdot e^{i{}^{\text{in}}\psi_{k-1}})\\&={}^{\text{out}}A_k\cdot e^{i{}^{\text{out}}\psi_k}-r\cdot {}^{\text{in}}A_k\cdot e^{i{}^{\text{in}}\psi_k}.\end{aligned}\tag{8}$$

After taking the absolute value on both sides of Eq. (8), the phase of the output pulse can be derived from

$${}^{\text{out}}\psi_k={}^{\text{in}}\psi_k\pm\arccos\left[\frac{r^2\cdot {}^{\text{in}}A_k^2+{}^{\text{out}}A_k^2-\alpha^2\cdot {}^{\text{in}}A_{k-1}^2-\alpha^2\cdot r^2\cdot {}^{\text{out}}A_{k-1}^2+2\alpha^2 r\cdot {}^{\text{in}}A_{k-1}\cdot {}^{\text{out}}A_{k-1}\cdot\cos({}^{\text{in}}\psi_{k-1}-{}^{\text{out}}\psi_{k-1})}{2r\cdot {}^{\text{in}}A_k\cdot {}^{\text{out}}A_k}\right].\tag{9}$$

Since the amplitude ${}^{\text{in}}A_k$ and the phase ${}^{\text{in}}\psi_k$ are input parameters, they can be treated as known variables. Pulses out of the cavity could be detected by a photodiode, which directly measures the pulse power, so one can get the pulse amplitude value from those power data. Given the parameters of ${}^{\text{in}}A_k$, ${}^{\text{in}}\psi_k$, and ${}^{\text{out}}A_k$, the phase of output pulse ${}^{\text{out}}\psi_k$ can be extracted from Eq. (9) if we have obtained the information of the $(k-1)^{th}$ pulse. Solving the cavity phase φ in Eq. (8), we conclude that

$$\varphi=\arg\left[\frac{{}^{\text{out}}A_k\cdot e^{i{}^{\text{out}}\psi_k}-r\cdot {}^{\text{in}}A_k\cdot e^{i{}^{\text{in}}\psi_k}}{\alpha(r\cdot {}^{\text{out}}A_{k-1}\cdot e^{i{}^{\text{out}}\psi_{k-1}}-{}^{\text{in}}A_{k-1}\cdot e^{i{}^{\text{in}}\psi_{k-1}})}\right],\tag{10}$$

where arg is a function giving the argument of a complex number. Equations (9) and (10) are basic formulas that extract the cavity and pulse phases from limited data.

More concretely, we calculate every output pulse phase ${}^{\text{out}}\psi_k$ iteratively from the first to the last equation in Eq. (7). Observing that cosine is an even function, generally we will find two solutions of ${}^{\text{out}}\psi_k$ from Eq. (9). According to Eq. (10), every iteration will generate a solution set consisting of four values of the cavity phase, which can be defined as a "vector" $(\varphi_{k1},\varphi_{k2},\varphi_{k3},\varphi_{k4})$. Fortunately, we can compare the solutions of the cavity phase provided by different iterations. The most likely value of the cavity phase is supposed to be one of the four candidates in every iteration, while the other three candidates (the least likely cavity phases) are extraneous solutions to Eq. (7). The probe pulse train should contain three or more pulses, which give us at least two vectors of cavity phases for comparison.

In the actual experiment, thermal drift, acoustic perturbation, mechanical vibration, and photodiode electronic noise will affect the calculation of the cavity phase. Since noise leads to the fluctuation of the calculated cavity phase, we introduce the definition of "distance" between two "cavity phase points" generated from two different iterations as

$$\delta_{\text{ka,lb}}=\min(|\varphi_{\text{ka}}-\varphi_{\text{lb}}|,2\pi-|\varphi_{\text{ka}}-\varphi_{\text{lb}}|),\tag{11}$$

where $k,\ l\in\{1,2,...,n\}$, $k\neq l$, and $a,\ b\in\{1,2,3,4\}$. In general, the most likely cavity phase points have the

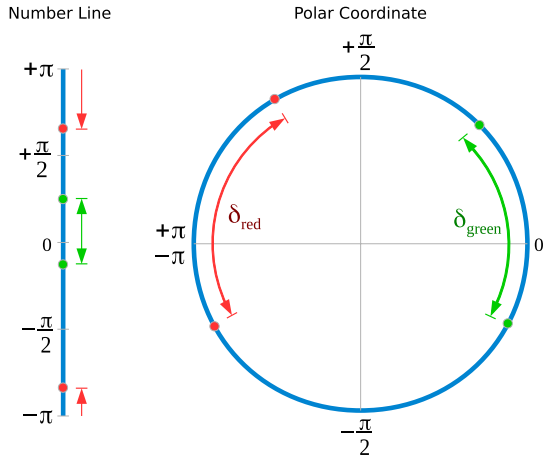

Fig. 2. Distance between cavity phase points.

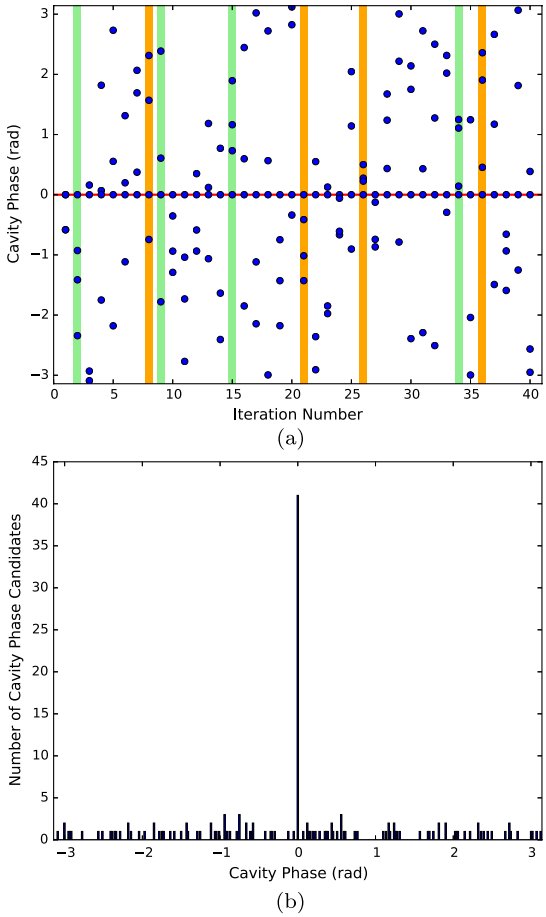

Fig. 3. (a) Four vectors (green or orange) are chosen randomly to extract the most likely cavity phase. The theoretical cavity phase (red) is 0 rad. (b) Histogram of all cavity phase candidates. The phase interval is 1.0°.

shortest distance to each other than the least likely cavity phase points. The distance definition within one cycle in radians can be treated as a "circular distance" shown in Fig. 2.

The impulse noise from one single pulse measurement will introduce the random error to our calculation. Implementing the random traversal in n vectors and using four vectors stochastically each time can mitigate the effect, as shown in Fig. 3(a). Counting the number of cavity phase candidates within a certain interval gives us a histogram, as shown in Fig. 3(b). The histogram indicates the distribution of all cavity phase candidates, and it illustrates that the most likely cavity phases from each iteration are located in the interval of the theoretical cavity phase and isolated from the least likely cavity phases. Since four vectors are chosen randomly to derive the most likely cavity phase, we define the distance among cavity phase points from four different vectors as

$$\delta = \delta_{\mathrm{ka,lb}} + \delta_{\mathrm{ka,pc}} + \delta_{\mathrm{ka,qd}} + \delta_{\mathrm{lb,pc}} + \delta_{\mathrm{lb,qd}} + \delta_{\mathrm{pc,qd}}, \quad (12)$$

where $k, l, p, q \in \{1, 2, \ldots, n\}$, k, l, p, q are not equal to each other, and $a, b, c, d \in \{1, 2, 3, 4\}$. Considering four vectors with four candidates in each vector, there will be 256 $(4 \times 4 \times 4 \times 4)$ distance values. If we could find the minimum from the 256 distance values, the corresponding cavity phase points are the most likely values of the cavity phases. Furthermore, phase unwrapping of the 2π complement has to be included in the calculation when dealing with the cavity phase near the boundary of $\pm\pi$. It is important to know that one can get the right pulse phase based on the one-to-one mapping between the pulse phase and the cavity phase in each iteration.

Based on the iteration formulas, we simulated the process of the CPS and extracted the cavity phase accurately from limited data accompanied by noise. In the actual experiment, low optical power levels require amplified and high-speed photodiodes that produce electronic noise. The simulation result shown in Fig. 4(a) is a pure system without noise in order to demonstrate the correctness of our algorithm, while the result shown in Fig. 4(b) implies the actual system with 1.0% power level noise. Stochastic values are applied to the input pulse amplitude and the input pulse phase for noise reduction. Averaging is also implemented in the calculation after extracting the most likely cavity phase values from each iteration. A simple initial calibration of the photodiode is needed beforehand to mitigate the nonlinearity.

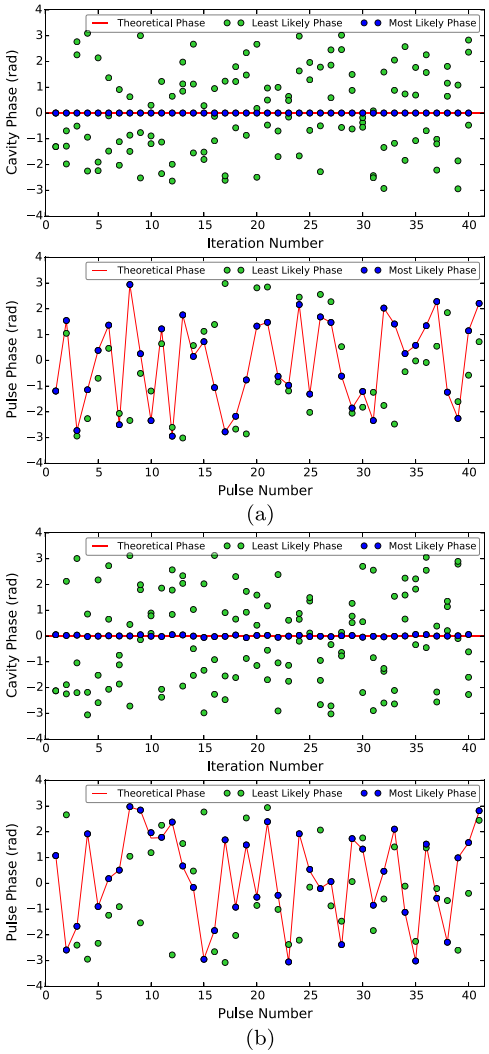

Fig. 4. Simulation results. The probe pulse train consists of 41 pulses. The cavity phase calculation needs 40 iterations. (a) Pure system without noise. (b) Actual system with 1.0% power level noise.

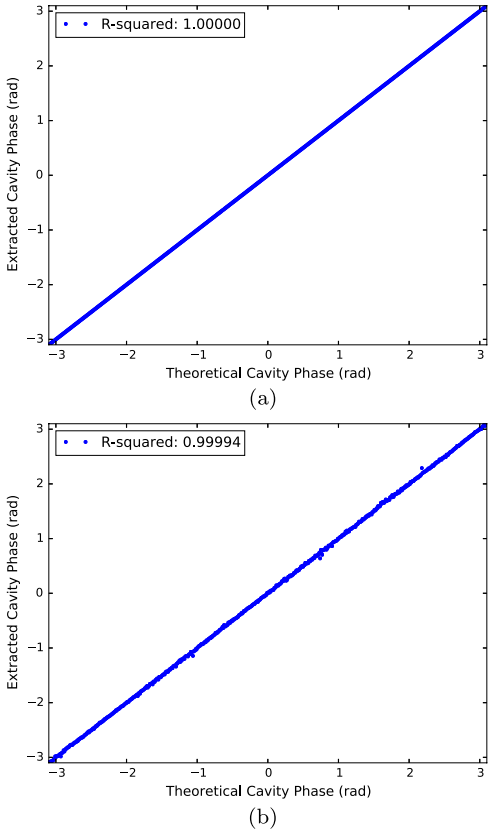

Fig. 5. Scanning the theoretical cavity phase over one cycle and extracting the most likely cavity phase accordingly. (a) Pure system without noise. (b) Actual system with 1.0% power level noise.

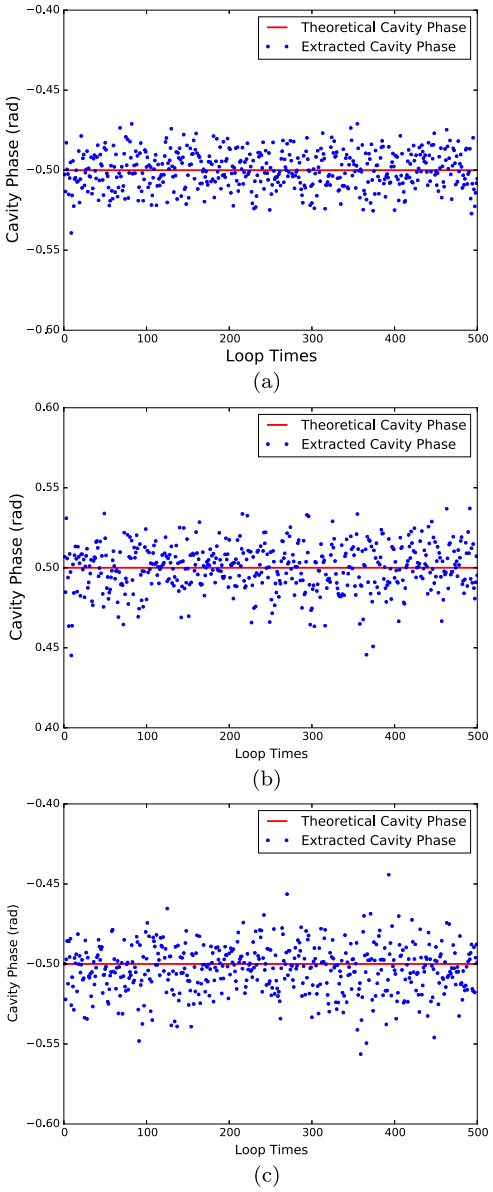

Fig. 6. Errors of extracted cavity phases in a three-cavity system. (a) Cavity phase error is 0.7° (RMS) in the first cavity. (b) Cavity phase error is 0.8° (RMS) in the second cavity. (c) Cavity phase error is 0.9° (RMS) in the third cavity.

As shown in Fig. 5, applying a ramp of theoretical cavity phase from $-\pi$ to π and extracting the resulting cavity phase illustrate that the algorithm is linear and isotropic in one phase cycle.

It is necessary to note that the output pulse train of the previous cavity can be used as the input pulse train of the next cavity. Properly cascading multiple optical cavities will achieve a high peak-power enhancement. Since the cavity phase and output pulse phases in one single optical cavity can be obtained completely according to the described algorithm, we can definitely extract all of the phase information (cavity phase and pulse phase) cavity by cavity with pulse amplitude data provided by photodiodes in the cascaded system of multiple cavities. We have implemented the described algorithm on a three-cavity system and simulated the calculation loop for 500 times. As shown in Fig. 6, cavity phases are extracted accurately with errors less than 1.0° [root mean square (RMS)] at 1.0% power level noise.

In conclusion, we have assembled a Z-transform model describing the optical interference process and an algorithm extracting the cavity phase and pulse phases from limited measurements, where only the intensity is available. We also have implemented the algorithm on the cascaded system of multiple optical cavities, achieving phase errors less than 1.0° (RMS). A simple initial calibration mitigating the photodiode nonlinearity is a necessary procedure before applying the algorithm to actual experiments.

This work was supported by the Director, Office of Science, Office of High Energy Physics, of the U.S. Department of Energy under Contract No. DE-AC02-05CH11231, and by the National Natural Science Foundation of China under Grant No. 11475097.

References

1. C. G. R. Geddes, C. Toth, J. van Tilborg, E. Esarey, C. Schroeder, D. Bruhwiler, C. Nieter, J. Cary, and W. P. Leemans, Nature **431**, 538 (2004).
2. W. Leemans and E. Esarey, Phys. Today **62**, 44 (2009).
3. R. Brinkmann, in *Proc. FEL 2006*, Berlin, Germany (2006), paper MOBAU03.
4. J. W. Dawson, M. J. Messerly, R. J. Beach, M. Y. Shverdin, E. A. Stappaerts, A. K. Sridharan, P. H. Pax, J. E. Heebner, C. W. Siders, and C.P.J. Barty, Opt. Express **16**, 13240 (2008).
5. T. Zhou, J. Ruppe, C. Zhu, I.-N. Hu, J. Nees, and A. Galvanauskas, Opt. Express **23**, 7442 (2015).
6. M. Kienel, M. Müller, A. Klenke, J. Limpert, and A. Tünnermann, Opt. Lett. **41**, 3343 (2016).
7. R. Wilcox, Y. Yang, D. Dahlen, Y. Xu, G. Huang, D. Qiang, L. Doolittle, J. Byrd, W. Leemans, J. Ruppe, T. Zhou, M. Sheikhsofla, J. Nees, A. Galvanauskas, J. Dawson, D. Chen, and P. Pax, in *Proc. AAC'16*, Oxon Hill, MD (2016).
8. J. Ruppe, H. Pei, M. Sheikhsofla, S. Chen, R. Wilcox, W. Leemans, J. Nees, and A. Galvanauskas, in *Proc. CLEO'17*, San Jose, CA, USA (2017), paper SM4I.1.
9. L. A. Siiman, W.-Z. Chang, T. Zhou, and A. Galvanauskas, Opt. Express **20**, 18097 (2012).
10. W. Z. Chang, T. Zhou, L. A. Siiman, and A. Galvanauskas, Opt. Express **21**, 3897 (2013).
11. M. Kienel, M. Müller, A. Klenke, T. Eidam, J. Limpert, and A. Tünnermann, Opt. Lett. **40**, 522 (2015).
12. F. Gires and P. Tournois, C. R. Hebd. Acad. Sci. **258**, 6112 (1964).
13. M. Sheikhsofla, J. Ruppe, J. Ness, D. Dahlen, R. Wilcox, and A. Galavanauskas, in *Proc. ASSL 2016*, Boston, USA (2016), paper AM4A.4.
14. M. Mueller, M. Kienel, A. Klenke, T. Eidam, J. Limpert, and A. Tünnermann, Opt. Express **24**, 7893 (2016).
15. Y. Yang, J. Byrd, J. Dawson, L. Doolittle, Q. Du, A. Galavanauskas, G. Huang, W. Leemans, J. Ruppe, R. Wilcox, and Y. Xu, in *Proc. CLEO'17*, San Jose, USA (2017), paper SM4I.3.
16. Y. Xu, R. Wilcox, J. Byrd, L. Doolittle, Q. Du, G. Huang, Y. Yang, T. Zhou, W. Leemans, A. Galavanauskas, J. Ruppe, C. Tang, and W. Huang, IEEE J. Quantum Electron. **54**, 1600111 (2018).